[Research Paper] 대한금속 · 재료학회지 (*Korean J. Met. Mater.*), Vol. 61, No. 3 (2023) pp.206-212
DOI: 10.3365/KJMM.2023.61.3.206

Electrical, Thermal, and Thermoelectric Transport Properties of Co-Doped *n*-type $Cu_{0.008}Bi_2Te_{2.6}Se_{0.4}$ Polycrystalline Alloys

Okmin Park[1,†], TaeWan Kim[2,†], Minsu Heo[1], Sang Jeong Park[1], Se Woong Lee[1], Hyun Kyu Cho[1], and Sang-il Kim[1,*]

[1]*Department of Materials Science and Engineering, University of Seoul, Seoul 02504, Republic of Korea*
[2]*Department of Electrical Engineering and Smart Grid Research Center, Jeonbuk National University, Jeonju 54896, Republic of Korea*

Abstract: Bi_2Te_3-based alloys have been extensively studied as thermoelectric materials near room temperature. In this study, the electrical, thermal, and thermoelectric transport properties of a series of Co-doped *n*-type $Cu_{0.008}Bi_2Te_{2.6}Se_{0.4}$ polycrystalline alloys ($Cu_{0.008}Bi_{2-x}Co_xTe_{2.6}Se_{0.4}$, x = 0, 0.03, 0.06, 0.09 and 0.12) are investigated. The electrical conductivity of the $Cu_{0.008}Bi_{1.97}Co_{0.03}Te_{2.6}Se_{0.4}$ (x = 0.03) sample was significantly enhanced, by 34%, to 1199 S/cm compared to 793 S/cm of the pristine $Cu_{0.008}Bi_2Te_{2.6}Se_{0.4}$ (x = 0) sample at 300 K, and gradually decreased to 906 S/cm for x = 0.12 upon further doping. Power factors of the Co-doped samples decreased compared to the 3.26 mW/mK^2 of the pristine $Cu_{0.008}Bi_2Te_{2.6}Se_{0.4}$ sample at 300 K. Meanwhile, the power factor of the $Cu_{0.008}Bi_{1.97}Co_{0.03}Te_{2.6}Se_{0.4}$ (x = 0.03) sample became higher at 520 K. The lattice thermal conductivities of the Co-doped samples decreased due to additional point defect phonon scattering by the Co dopant. Consequently, the zT for the $Cu_{0.008}Bi_{1.97}Co_{0.03}Te_{2.6}Se_{0.4}$ alloy at 520 K was 0.83, which is approximately 15% larger than that of pristine $Cu_{0.008}Bi_2Te_{2.6}Se_{0.4}$, while the zT of the Cu doped samples at 300 K was smaller than that of the pristine $Cu_{0.008}Bi_2Te_{2.6}Se_{0.4}$ sample. Electrical transport properties of the Co-doped $Cu_{0.008}Bi_{2-x}Co_xTe_{2.6}Se_{0.4}$ samples were analyzed by experimental phenomenological parameters, including the density-of-state, effective mass, weighted mobility, and quality factor.

(Received 5 December, 2022; Accepted 20 December, 2022)

Keywords: thermoelectric, Bi_2Te_3, doping

1. INTRODUCTION

Bi_2Te_3-based alloys have been extensively studied as thermoelectric materials at room temperature. These materials are semiconductors with a narrow band gap (~ 0.13 eV) [1,2]. They have excellent electrical transport properties with a high carrier concentration (~ 10^{19} cm^{-3}) and exhibit a relatively low thermal conductivity due to layered structures with a weak Van der Waals bonding between layers [3-5], resulting in a good thermoelectric figure of merit (zT) at room temperature [6,7]. Thermoelectric performance is evaluated by the dimensionless Figure of merit, $zT = S^2\sigma T/\kappa_{tot}$, where S, σ, T, and κ_{tot} are Seebeck coefficient, electrical conductivity, absolute temperature, and total thermal conductivity ($\kappa_{tot} = \kappa_{ele} + \kappa_{latt}$, where κ_{ele} and κ_{latt} are electron and lattice thermal conductivities, respectively), respectively. At elevated temperatures Bi_2Te_3-based alloys also induce an intrinsic excitation of electron-hole pairs, resulting in a decrease in S and an increase in κ_{tot}. Therefore, Bi_2Te_3-based alloys exhibit rapidly degrading thermoelectric performance above 500 K [8-10], which limits the application of Bi_2Te_3 alloys to low temperatures, of 450 K or less.

Pristine Bi_2Te_3 is an n-type semiconductor and is typically doped with Se into the Te-site to improve its thermoelectric performance. However, Bi_2Te_3 compositions exhibit unstable carrier transport properties because of self-defects, the formation of anti-site defects, and Te-site vacancies [11]. The unstable carrier transport properties of n-type $Bi_2Te_{3-x}Se_x$ can be stabilized by adding Cu [12-15].

†These authors contributed equally to this study.
- 박옥민: 석사과정, 허민수 · 박상정 · 이세웅 · 조현규: 학부과정, 김태완 · 김상일: 부교수
**Corresponding Author:* Sang-il Kim
[Tel: +82-, E-mail: sang1.kim@uos.ac.kr]

Defect engineering, such as doping, addition, and solid-solution, are the most used strategies for reducing κ_{latt} by promoting point defect phonon scattering [16-19]. Doping strategies have been widely applied to enhance the thermoelectric transport properties of thermoelectric materials, particularly the n-type Bi_2Te_3-based alloys [19-22]. Lee et al. reported that using I-doping to improve the carrier transport properties of $Cu_{0.008}Bi_2Te_{2.7}Se_{0.3}$ enhanced zT to 0.86 at 400 K [21]. A higher zT of 1.07 at 423 K was observed in CuI-doped $Bi_2Te_{2.7}Se_{0.3}$ processed by hot–deformation [22]. Similarly, Co doping was used to enhance the electrical transport properties of pristine Bi_2Te_3 and p-type $Bi_{0.5}Sb_{1.5}Te_3$ [23,24].

However, Co-doping to $Bi_2Te_{3-x}Se_x$, a representative type of n-type Bi_2Te_3 based alloy, has not yet been reported. Therefore, in this study, the electrical, thermal, and thermoelectric transport properties of $Cu_{0.008}Bi_{2-x}Co_xTe_{2.6}Se_{0.4}$ (x = 0, 0.03, 0.06, 0.09 and 0.12) polycrystalline bulk alloys were investigated. The electrical transport properties of a Co-doped $Cu_{0.008}Bi_{2-x}Co_xTe_{2.6}Se_{0.4}$ composition were analyzed by experimental phenomenological parameters, including the density-of-state effective mass (m_d^*), weighted mobility (μ_w), and quality factor (B).

2. EXPERIMENTAL

Polycrystalline $Cu_{0.008}Bi_{2-x}Co_xTe_{2.6}Se_{0.4}$ (x = 0, 0.03, 0.06, 0.09 and 0.12) samples were prepared via the solid-state reaction method. Stoichiometric ratios of high purity Bi (99.999%, 5N Plus), Te (99.999 %, 5N Plus), and Co (99.99%, Sigma Aldrich) were sealed in a quartz tube under a pressure of 10^{-5} Torr to prevent oxidation or other reactions with air. The raw materials placed in the sealed quartz ampoules were synthesized at 1323 K for 12 h (heating rate of 3 K/min), and then slowly cooled in a box furnace. The synthesized ingots were pulverized for 5 min via high energy ball milling (SPEX 8000D, SPEX) in an Ar atmosphere. The powders placed in the graphite molds were sintered using spark plasma sintering (SPS-1030, Sumitomo Coal Mining Co., Ltd.) under 10^{-6} Torr at 707 K for 5 min (heating rate = 100 K/min) under 70 MPa. The sintered bulk samples had relative densities of more than ~ 99%.

X-Ray diffraction (XRD, D8 Discover, Bruker) analysis was performed to analyze the crystal structure of the samples. The polycrystalline powder samples were excited with 0.154 nm wavelength Cu–Kα radiation. For the σ and S measurements, the sintered samples were processed into rectangular shapes with dimensions of 2 mm × 2 mm × 8 mm. The processed specimens were analyzed using ZEM-3 (Advanced-Riko) in the temperature range 300–520 K in a He atmosphere, and the power factor was calculated using the measured σ and S. The Hall carrier concentrations (n_H) and Hall carrier mobilities (μ_H) were measured using a Hall measurement system (HMS5300, Ecopia) under a magnetic field of 0.548 T; the Hall measurements were performed using the van der Pauw configuration. The laser flash method (LFA457, Netzsch) was performed to obtain the thermal diffusivity (α) required to calculate κ_{tot} ($\kappa_{tot} = \alpha \times \rho_s \times C_p$, where ρ_s and C_p are the sample density and heat capacity, respectively). The ρ_s value is the theoretical density of $Bi_2Te_{2.6}Se_{0.4}$ —assuming a linear increase in the Bi_2Te_3 (7.834 g/cm^3)–Bi_2Se_3 (7.664 g/cm^3) system. The C_p value of Bi_2Te_3 was determined from the empirical formulas of $108.06 + 5.53 \times 10^{-2}$ T J/mol·K and C_p of $Bi_2Se_3 = 118.61 + 1.92 \times 10^{-2}$ T J/mol·K [25]. The zT value was evaluated using the calculated power factor and κ_{tot}.

3. RESULTS AND DISCUSSION

The XRD patterns for the $Cu_{0.008}Bi_{2-x}Co_xTe_{2.6}Se_{0.4}$ powder samples indicated a single rhombohedral Bi_2Te_3 phase without any additional phases (Figure 1(a)). The lattice parameters, a and c were calculated using the (015) and (1010) diffraction peaks (Figure 1(b)). The calculated lattice parameters gradually decreased with an increase in x values; a decreased from 4.365 to 4.348 Å and c decreased from 30.390 to 30.323 Å. This is because Co is substituted and doped at the Bi–site, that is, a Co-cation (~ 88.5 pm) with a relatively small ionic radius replaced the Bi^{+3} (117 pm).

Figures 2(a) and 2(b) show σ and S as a function of temperature, respectively, for the polycrystalline bulk samples along the direction perpendicular to the sintering pressure. The σ values of the Co-doped samples were higher than those of the undoped sample at all temperature ranges, and all samples exhibited intrinsic metal behavior. As shown in the inset of Figure 2(a), the σ values for x = 0, 0.03, 0.06,

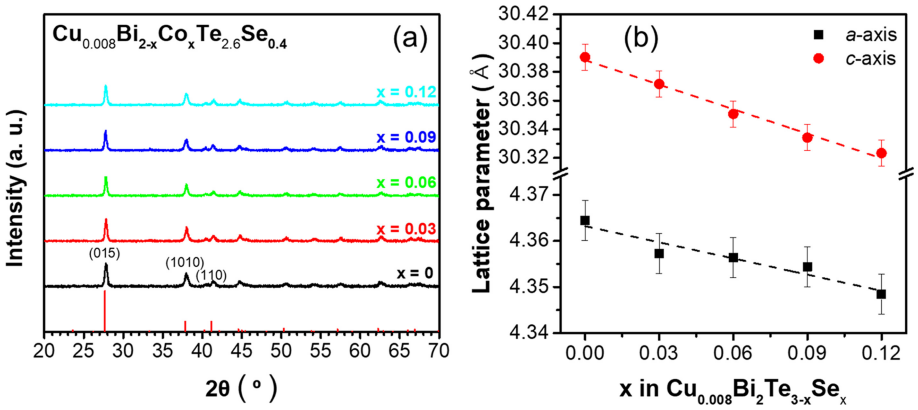

Fig. 1. (a) XRD patterns and (b) lattice parameters of the $Cu_{0.008}Bi_{2-x}Co_xTe_{2.6}Se_{0.4}$ (x = 0, 0.03, 0.06, 0.09 and 0.12) polycrystalline bulk alloys.

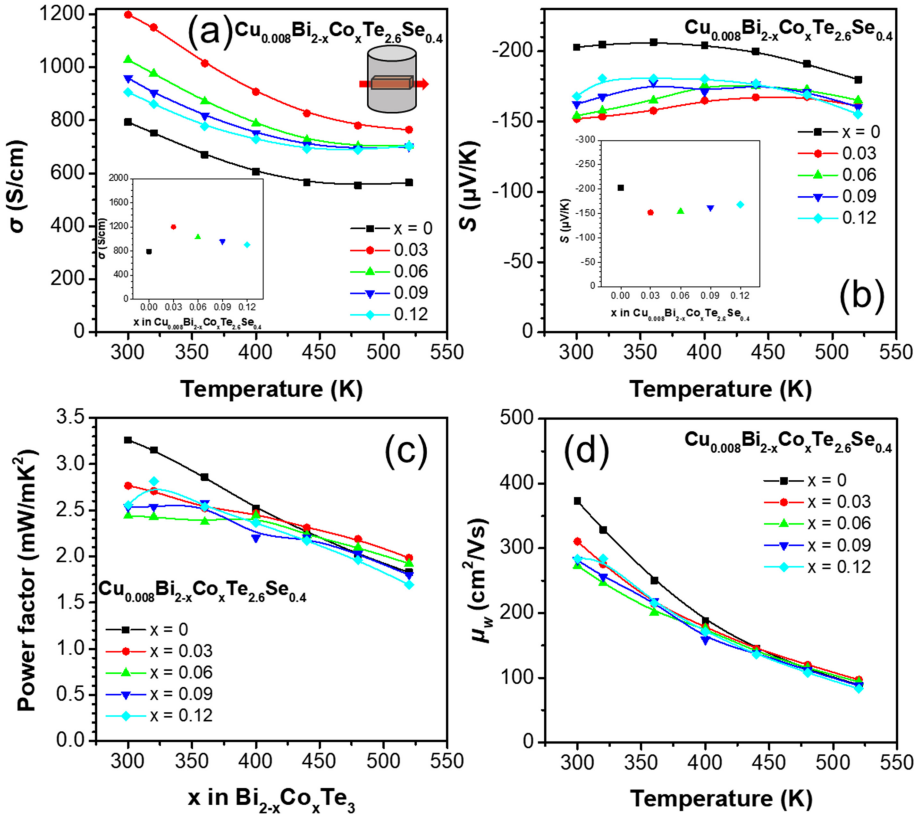

Fig. 2. (a) σ, (b) S, (c) power factor, and (d) μ_w as a function of the temperature for the $Cu_{0.008}Bi_{2-x}Co_xTe_{2.6}Se_{0.4}$ (x = 0, 0.03, 0.06, 0.09 and 0.12) polycrystalline bulk alloys. Insets of (a) σ and (b) S as a function of x content at 300 K.

0.09, and 0.12 were 793, 1199, 1028, 960, and 906 S/cm, respectively, at 300 K. Remarkably, the σ values systemically decreased with increases in doping level, after abruptly increasing at x = 0.03. The S values were similar even with the increase in temperature with a decrease in the doped samples, owing to the trade-off relationship between σ and S. Therefore, the S values showed the opposite trend compared to σ. The S values for x = 0, 0.03, 0.06, 0.09, and 0.12 were −202, −152, −154, −163, and −168 μV/K (inset of Figure 2(b)), respectively, at 300 K.

Figures 2(c) and 2(d) present the calculated power factor and weighted mobility μ_w as a function of temperature for the

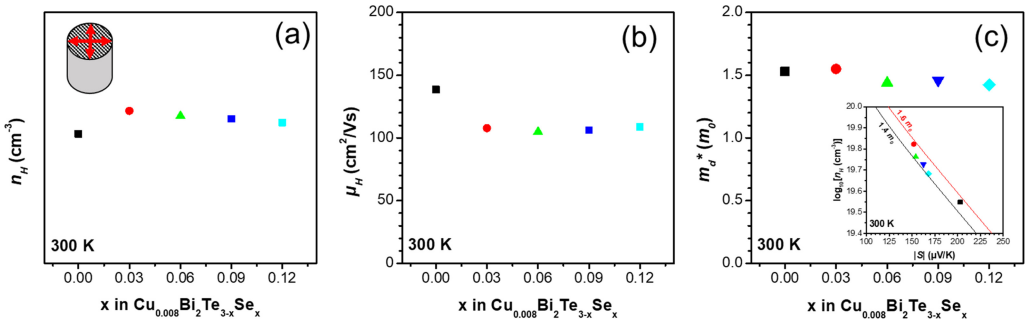

Fig. 3. (a) n_H and (b) μ_H (c) m_d^* as a function of the x content for the $Cu_{0.008}Bi_{2-x}Co_xTe_{2.6}Se_{0.4}$ ($x = 0$, 0.03, 0.06, 0.09 and 0.12) polycrystalline bulk alloys. Inset of (c) $\log_{10}(n_H)$ as a function of $|S|$ at 300 K.

$Cu_{0.008}Bi_{2-x}Co_xTe_{2.6}Se_{0.4}$ samples. As shown in Figure 2(c), the power factor for the samples decreased with the increase in temperature. The power factor of the doped samples decreased in the temperature range of 300–400 K compared to the undoped sample. However, after 450 K, the $x = 0.03$ and 0.06 samples showed a reverse trend; the power factor of the $x = 0.03$ sample increased by approximately 10% compared to the undoped sample at 520 K. The power factor values of the $x = 0$, 0.03, and 0.06 samples were 1.83, 1.99, and 1.92 mW/mK^2 at 520 K, respectively. The maximum power factor was 3.26 mW/mK^2 for the $x = 0$ sample at 300 K. The μ_w value was obtained from a simple analytical form that approximates the exact Drude–Sommerfeld free-electron model given in Equation (1) for $|S| > 20$ μV/K [26].

$$\mu_w = \frac{3h^3\sigma}{8\pi e(2m_e kT)^{3/2}}$$

$$\left[\frac{\exp\left[\frac{|S|}{k/e}-2\right]}{1+\exp\left[-5\left(\frac{|S|}{k/e}-1\right)\right]}+\frac{\frac{3}{\pi^2}\frac{|S|}{k/e}}{1+\exp\left[5\left(\frac{|S|}{k/e}-1\right)\right]}\right] \quad (1)$$

where k, m_e, e, and h are the Boltzmann constant, mass of the electron, elementary charge, and Planck's constant, respectively. The μ_w parameter infers the maximum reachable power factor when n_H is optimized. The μ_w value of each sample was evaluated using the measured σ and S parameters; the μ_w values showed a similar trend as the power factor. The maximum μ_w value was 373 cm^2/Vs for the $x = 0$ sample at 300 K.

Figure 3(a) shows n_H as a function of x for the $Cu_{0.008}Bi_{2-x}Co_xTe_{2.6}Se_{0.4}$ samples along the direction perpendicular to the sintering pressure. The n_H values showed a trend similar to the σ values; n_H increased approximately twice for the $x = 0.03$ (6.66×10^{19} cm^{-3}) sample compared to the $x = 0$ (3.54×10^{19} cm^{-3}) sample at 300 K and then decreased linearly with increases in x. The μ_H values for the Co-doped samples decreased because μ_H is inversely proportional to n_H; however, unlike n_H, the μ_H values were constant after $x = 0.06$ (Figure 3(b)). The μ_H values for the $x = 0$, 0.03, 0.06, 0.09, and 0.12 samples are 139 108, 105, 106, and 109 cm^2/Vs at 300 K, respectively.

The magnitude of the density of states is directly related to the density-of-state effective mass m_d^* and the electrical transport behavior was interpreted in terms of changes in the electron structure by calculating m_d^*. Equation (2), which was optimized to a single parabolic band model, is used to plot m_d^* for the samples (Figure 3(c)) [27].

$$\log_{10}\left(\frac{m_d^* T}{300}\right) = \frac{2}{3}log_{10}(n) - \frac{2}{3}[20.3 - (0.00508 \times |S|) + (1.58 \times 0.967^{|S|})] \quad (2)$$

The m_d^* value of the $x = 0.03$ (1.55 m_0) sample was larger than that of the $x = 0$ (1.529 m_0) sample at 300 K because m_d^* is proportional to both $|S|$ and n_H. This indicates that the decrease in $|S|$ for the $x = 0.03$ sample is less than the increase in n_H at 300 K. The inset of Figure 3(c) shows a plot of $\log_{10}(n_H)$ as a function of $|S|$ for the samples. The m_d^* becomes generally lower with the Co doping.

Figure 4(a) shows κ_{tot} as a function of temperature for the

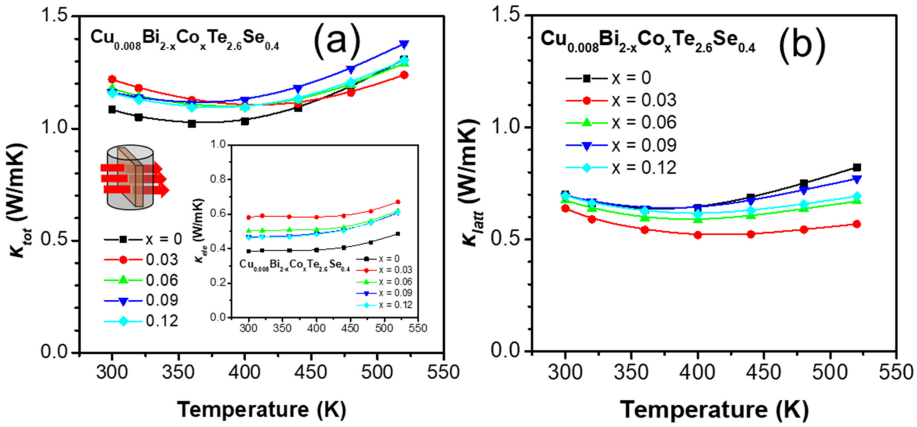

Fig. 4. (a) κ_{tot} and (b) κ_{latt} as a function of temperature for the $Cu_{0.008}Bi_{2-x}Co_xTe_{2.6}Se_{0.4}$ (x = 0, 0.03, 0.06, 0.09 and 0.12) polycrystalline bulk alloys. Inset of (a) κ_{ele} as a function of temperature.

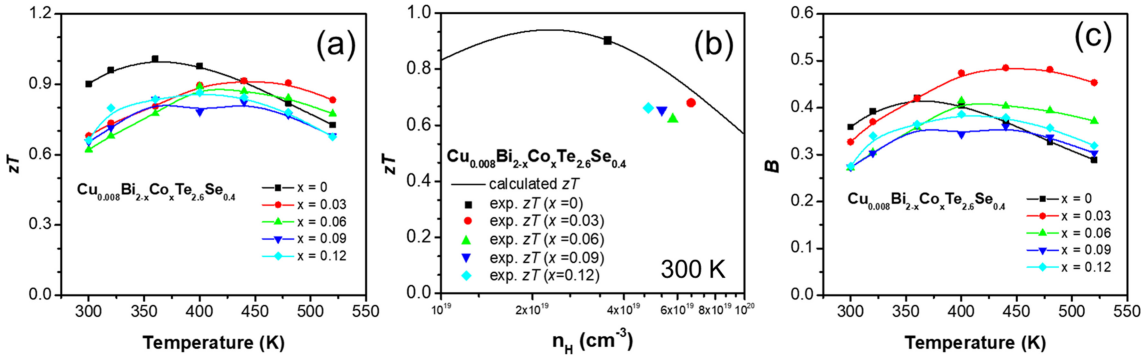

Fig. 5. (a) zT as a function of temperature for the $Cu_{0.008}Bi_{2-x}Co_xTe_{2.6}Se_{0.4}$ (x = 0, 0.03, 0.06, 0.09 and 0.12) polycrystalline bulk alloys. (b) n_H-dependent experimental zT (denoted using symbols) of $Cu_{0.008}Bi_{2-x}Co_xTe_{2.6}Se_{0.4}$ (x = 0, 0.03, 0.06, 0.09, and 0.12) and calculated zT (denoted using a line) via single parabolic band model. (c) B as a function of temperature for the $Cu_{0.008}Bi_{2-x}Co_xTe_{2.6}Se_{0.4}$ (x = 0, 0.03, 0.06, 0.09, and 0.12) polycrystalline bulk alloys.

$Cu_{0.008}Bi_{2-x}Co_xTe_{2.6}Se_{0.4}$ samples along the direction perpendicular to the sintering pressure. The κ_{tot} values of the x = 0.03, 0.06, 0.09, and 0.12 samples at 300–450 K increased with the increase in κ_{ele} (inset of Figure 4(a)). The κ_{ele} values were calculated using $\kappa_{ele} = L\sigma T$ (where L is the Lorenz number [28]) and the increase in κ_{tot} significantly affected the increase in σ of the Co-doped samples. Therefore, the values of κ_{tot} for the x = 0, 0.03, 0.06, 0.09, and 0.12 samples at 300 K were 1.08, 1.22, 1.18, 1.16, and 1.16 W/mK, respectively, In contrast, the κ_{tot} values of the x = 0.03, 0.06, and 0.12 samples at 520 K decreased to 1.24, 1.29, and 1.31 W/mK, respectively, from that of the x = 0 (1.31 W/mK at 520 K) sample. Interestingly, the κ_{latt} reached its lowest value at x = 0.03, and increased for the higher doping samples. The physical reason behind the unusual observation for κ_{latt} may be the complex defect structures produced by the Co doping, which requires further study.

Figure 5(a) illustrates the zT of the $Cu_{0.008}Bi_{2-x}Co_xTe_{2.6}Se_{0.4}$ polycrystalline bulk samples. The thermoelectric performance of the Co-doped samples significantly decreased in contrast to the undoped sample at 300 K. The maximum zT value of the undoped sample at 300 K was 1.0. However, the zT of the undoped sample decreased above 360 K, while those of the x = 0.03 and 0.06 samples marginally increased above 450 K. Therefore, the zT values of x = 0.03 and 0.06 were enhanced more than the x = 0 sample at 480 and 520 K. The zT values of the x = 0.03, and 0.06 samples were 0.91, and 0.84 at 480 K and 0.83, and 0.77 at 520 K, respectively. Further, the zT values of the x = 0.03 and 0.06 samples were enhanced to approximately 8% and 3% at 480 K and to approximately 15% and 7% at 520 K, compared with the x = 0 (0.82 and 0.72 at 480 and 520 K, respectively), respectively.

Figure 5(b) shows the n_H-dependent zT calculated via the single parabolic band model and experimental zT at 300 K; n_H-dependent experimental zT (denoted using symbols) and calculated zT (denoted using a line), which indicates the theoretically achievable zT at 300 K. The zT values of all the Co-doped samples were lower than the achievable zT (line in Figure 5(b)), which would infer the band structure was unfavorably changed by the doping. Because the n_H value of the $x = 0.03$ sample was the highest, it is plotted at the rightmost side (n_H of 6.7 ×10^{19} cm^{-3}) in the graph (solid red). As the doping content increases, the symbols shift toward the left, which indicates a decrease in n_H. However, the peak value of the calculated zT was observed when n_H was 2.2 × 10^{19} cm^{-3}. Therefore, n_H optimization of the samples is required. Based on the calculation, shown in Fig. 5(b), zT can be increased to 0.94 at 300 K when n_H is optimized (decreased) to ~ 2.2 × 10^{19} cm^{-3}. Dopants to decrease the mother compound $Cu_{0.008}Bi_2Te_{2.6}Se_{0.4}$ could be introduced to enhance zT at 300 K.

Figure 5(c) shows the dimensionless thermoelectric quality factor B, which was evaluated using Equation (3) [26]:

$$B = \left(\frac{k}{e}\right)^2 \frac{8\pi e(2m_e kT)^{3/2}}{3h^3} \cdot \frac{\mu_w}{\kappa_{latt}} T \quad (3)$$

Based on previous studies, B is proportional to the maximum zT value that can be achieved for an optimized n_H [29, 30]. Therefore, the general trend of B is similar to that of zT; however, in this study, the x=0.03 sample has a maximum B value (0.49) at 440 K. In particular, the B values for all doped samples above 480 K were less than that of the undoped sample. The B values of the $x = 0$, 0.03, 0.06, 0.09, and 0.12 samples were 0.29, 0.45, 0.37, 0.30, and 0.32, respectively, at 520 K. This indicates that in the Co-doped samples at 520 K, zT can be increased to a greater extent, when n_H is optimized.

4. CONCLUSIONS

In summary, the thermoelectric properties of Co-doped $Bi_2Te_{2.6}Se_{0.4}$, $Cu_{0.008}Bi_{2-x}Co_xTe_{2.6}Se_{0.4}$ ($x = 0$, 0.03, 0.06, 0.09, and 0.12) polycrystalline samples were investigated. The electrical conductivity generally increased for the Co-doped samples and the S values decreased. The measured power factor of the Co-doped samples was lower than 3.26 mW/mK^2 for the pristine $Cu_{0.008}Bi_2Te_{2.6}Se_{0.4}$ sample at 300 K. However, the power factor of the $Cu_{0.008}Bi_{1.97}Co_{0.03}Te_{2.6}Se_{0.4}$ ($x = 0.03$) sample became higher at 520 K. A decrease in lattice thermal conductivity was observed for the Co-doped samples due to additional point defect phonon scattering. Consequently, a maximum zT of 1.0 was observed for the $x = 0$ sample at 300 K; however, above 440 K, the zT values of the $x = 0.03$ and 0.06 samples were approximately 15% and 7% larger than that of the $x = 0$ sample, at 520 K, respectively. Furthermore, a maximum quality factor of 0.49 was observed for the $x = 0.03$ sample at 440 K, which would infer that the highest zT can be obtained with the $x = 0.03$ sample at 440 K by optimizing carrier concentration.

Conflict of interest statement

There is no conflict of interest.

ACKNOWLEDGEMENT

This study was supported by the National Research Foundation of Korea (NRF-2019R1C1C1005254 and NRF-2022R1F1A1063054).

REFERENCES

1. O. Madelung, Semiconductors: Data Handbook, *Springer Science & Business Media* (2004).
2. G. S. Nolas, J. Sharp, and H. J. Goldsmid, Thermoelectrics: Basic Principles and New Materials Developments, *Springer Science & Business Media* (2001).
3. A. Taylor, C. Mortensen, R. Rostek, N. Nguyen, and D. C. Johnson, *J. Electron. Mater.* **39**, 1981 (2010).
4. Y. L. Chem, J. G. Analytis, J.-H. Chu, Z. K. Liu, S.-K. Mo, X. L. Qi, H. J. Zhang, D. H. Lu, X. Dai, Z. Fang, S. C. Zhang, I. R. Fisher, Z. Hussain, AND Z.-X. Shen, *Science* **325**, 178 (2009).
5. W. Yuan, L. Wei-Di, G. Han, W. Li-Jun, L. Meng, S. Xiao-Lei, H. Min, W. Hao, Z. Jin, C. Zhi-Gang, *ACS Appl. Mater. & Interfaces* **11**, 31237 (2019).
6. B. Poudel, Q. Hao, Y. Ma, Y. Lan, A. Minnich, B. Yu, X. Yan, D. Wang, A. Muto, D. Vashaee, X. Chen, J. Liu, M. S. Dresselhaus, G. Chen, and Z. Ren, *Science* **320**, 634 (2008).

7. S. I. Kim, K. H. Lee, H. A. Mun, H. S. Kim, S. W. Hwang, J. W. Roh, D. J. Yang, W. H. Shin, X. S. Li, Y. H. Lee, G. J. Snyder, and S. W. Kim, *Science* **348**, 109 (2015).
8. K. H. Lee, W. H. Shin, H. S. Kim, H. J. Cho, S. W. Kim, and S. I. Kim, *Scr. Mater.* **186**, 225 (2020).
9. F. Hao, T. Xing, P. Qiu, P. Hu, T. Wei, D. Ren X. Shi, and L. Chen, *ACS Appl. Mater. & Interfaces*, **10**, 21372 (2018).
10. L.-P. Hu, T.-J. Zhu, Y.-G. Wang, H.-H. Xie, Z.-J. Xu, and X.-B. Zhao, *NPG Asia Mater.* **6**, e88 (2014).
11. J. Jiang, L. Chen, S. Bai, Q. Yao, and Q. Wang, *Mater. Sci. Eng. B Solid-State Mater. Adv. Technol.* **117**, 334 (2005).
12. K. H. Lee, Y. Kim, D. H. Kim, C. O. Park, H.-S. Kim, and S.-i. Kim, *J. Mater. Res. Technol-JMRT.* **15**, 4781 (2021).
13. Y. H. Kim, Y. Kim, H.-S. Kim, S.-M. Choi, S.-i. Kim, and K. H. Lee, *Int. J. Energy Res.* **46**, 3707 (2022).
14. H.-J. Cho, H.-S. Kim, W.-h. Sohn, and S.-i. Kim, *Korean J. Met. Mater.* **58**, 439 (2020).
15. Y.-M. Kim, K. H. Lee, L. Fu, M.-W. Oh, S.-H. Yang, S. Ning, G. Hana, M. Y. Kim, J.-S. Kim, M. Jeong, J. Jang, E. Lee, E. Okunishi, H. Sawada, S.-i. Kim, S. J. Pennycook, Y. H. Lee, and S. W. Kim, *Mater. Today Phys.* **17**, 100347 (2021).
16. L. Hu, T. Zhu, X. Liu, and X. Zhao, *Adv. Funct. Mater.* **24**, 5211 (2014).
17. K. H. Lee, Y.-M. Kim, C. O. Parka, W. H. Shin, S. W. Kim, H.-S. Kim, and S.-i. Kim, *Mater. Today Energy* **21**, 100795 (2021).
18. S. W. Lee, O. Park, H.-S. Kim, W.-S. Seo, S.-i. Kim, *Korean J. Met. Mater.* **60**, 919 (2022).
19. O. Park, T. Kim, S. W. Lee, H.-s. Kim, W. H. Shin, J. U. Rahman, and S.-i. Kim, *Korean J. Met. Mater.* **60**, 315 (2022).
20. S. Jo, H.-S. Kim, Y. Kim, S.-i. Kim, and K. H. Lee, *J. Alloys Compd.* **884**, 161030 (2021).
21. K. H. Lee, H.-S. Kim, S.-S. Choo, W. H. Shin, J.-H. Lim, S. W. Kim, and S.-i. Kim, *Scr. Mater.* **186**, 357 (2020).
22. L. Hu, T. Zhu, X. Liu, and X. Zhao, *Adv. Funct. Mater.* **24**, 5211 (2014).
23. Z. Wei, C. Wang, J. Zhang, J. Yang, Z. Li, Q. Zhang, P. Luo, W. Zhang, E. Liu, and J. Luo, *ACS Appl. Mater. Interfaces* **12**, 20653 (2020).
24. P. Singha, S. Das, V. A. Kulbashinskii, V. G. Kytin, S. Chakravarty, A. K. Deb, S. Bandyopadhyay, and A. Banerjee, *Int. J. Energy Res*. **46**, 17029 (2022).
25. K. C. Mills, *Thermodynamic data for inorganic sulphides, selenides and tellurides*, pp. 845, Butterworths, London (1974).
26. G. J. Snyder, A. H. Snyder, M. Wood, R. Gurunathan, B. H. Snyder, and C. Niu, *Adv. Mater.* **32**, 2001537 (2020).
27. K. H. Lee, S.-i. Kim, J.-C. Lim, J. Y. Cho, H. Yang, and H.-S. Kim, *Adv Funct Mater*. **32**, 2203852 (2022).
28. H. S. Kim, Z. M. Gibbs, Y. Tang, H. Wang, and G. J. Snyder, *APL Mater.* **3**, 041506 (2015).
29. Y. Pei, H. Wang, and G. J. Snyder, *Adv Mater*. **24**, 6125 (2012).
30. J. Xin, Y. Tang, Y. Liu, X. Zhao, H. Pan, and T. Zhu, *npj Quantum Mater*. **3**, 1 (2018).